minerals

MDPI

Article

Geochemical Characteristics and Hydrocarbon Generation Potential of Source Rocks in the Shanxi and Taiyuan Formations, Qingyang Gas Field

Ruitao Yan [1], Chao Ye [2], Chao Li [2], Yu Zhang [2], Yaxin Duan [2], Yuanyuan Kou [2] and Zhaobing Chen [3,*]

[1] College of Petroleum Engineering, Xi'an Shiyou University, Xi'an 710065, China; yanruitao@xsyu.edu.cn
[2] Second Oil Production Plant, PetroChina Changqing Oilfield Company, Qingyang 745100, China; yechao_cq@petrochina.com.cn (C.Y.); lichao01_cq@petrochina.com.cn (C.L.); zyu01_cq@petrochina.com.cn (Y.Z.); duanyaxin_cq@petrochina.com.cn (Y.D.); kouyy_cq@petrochina.com.cn (Y.K.)
[3] School of Earth Science and Engineering, Xi'an Shiyou University, Xi'an 710065, China
* Correspondence: zbchen@xsyu.edu.cn

Abstract

To clarify the hydrocarbon-generation potential of deep source rocks in the Qingyang Gas Field, this study focuses on the Shanxi and Taiyuan Formation source rocks at burial depths of 4000–5000 m. Integrated organic geochemical analyses were conducted to investigate organic matter abundance, kerogen type, thermal maturity, hydrocarbon-generation conditions, and their significance for natural gas accumulation. The TOC values of the 12 valid mudstone samples range from 0.07% to 2.53%, with an average of 0.77%, indicating generally poor to fair organic matter abundance. Rock-Eval results show that S2 values range from 0.0681 to 6.2797 mg/g, with an average of 1.5946 mg/g, whereas S1 + S2 values range from 0.0948 to 6.9066 mg/g, with an average of 1.8582 mg/g, indicating generally limited Rock-Eval hydrocarbon-generating capacity, with local improvement. The kerogen assemblage is heterogeneous and is generally dominated by Type III humic kerogen, with subordinate Type II components and minor Type I components in some samples, indicating mixed organic-matter input but an overall gas-prone character. Tmax values range from 420 to 482 °C; however, because Tmax may be unreliable in samples with very low S2 values, thermal maturity was evaluated mainly using vitrinite reflectance and natural gas geochemical evidence. R_o values range from 2.03% to 2.22%, with an average of 2.11%, indicating that the source rocks have reached a high- to overmature stage. The natural gas is methane-rich, with an average methane content of 91.73% and an average heavy hydrocarbon content of only 0.16%, indicating a typical dry-gas composition. The carbon isotope values of methane and ethane are both negative, with $\delta^{13}C_1$ values ranging from −35.59‰ to −20.65‰ and $\delta^{13}C_2$ values ranging from −37.82‰ to −28.44‰, consistent with high-maturity coal-derived gas generated from humic organic matter. The formation water is mainly medium- to high-salinity $CaCl_2$ type, indicating a relatively closed hydrologic environment favorable for natural gas preservation. Clay mineral assemblages dominated by kaolinite and illite provide supplementary evidence for depositional conditions, burial diagenesis, and fluid–rock interaction. Overall, although the Rock-Eval hydrocarbon-generating capacity of the Shanxi and Taiyuan Formation source rocks is generally limited, the Type III-dominated mixed kerogen, high- to overmature R_o values, methane-rich dry-gas composition, and carbon isotope characteristics collectively indicate that these source rocks experienced effective natural gas generation during geological evolution and are genetically related to the present deep natural gas accumulation. This study provides fundamental geochemical constraints for further integrated exploration and evaluation of the deep coal-measure gas system in the Qingyang Gas Field.

Check for updates

Academic Editor: Thomas Gentzis

Received: 2 April 2026
Revised: 4 May 2026
Accepted: 19 May 2026
Published: 21 May 2026

Copyright: © 2026 by the authors. Licensee MDPI, Basel, Switzerland. This article is an open access article distributed under the terms and conditions of the Creative Commons Attribution (CC BY) license.

Keywords: Ordos Basin; Qingyang gas field; Shanxi and Taiyuan formations; source rock; organic geochemical characteristics; hydrocarbon generation potential; reservoir conditions

1. Introduction

Source-rock characterization is a fundamental component of petroleum system analysis and hydrocarbon resource evaluation. In different petroliferous basins worldwide, integrated organic geochemical approaches, including total organic carbon (TOC), Rock-Eval pyrolysis, kerogen petrography, vitrinite reflectance, biomarker parameters, and stable carbon isotopes, have been widely used to evaluate organic matter abundance, quality, thermal maturity, depositional environment, and hydrocarbon-generation potential. Previous studies from the Upper Indus Basin, northern Iraq, and the onshore and offshore basins of Yemen have demonstrated that source-rock assessment requires the integration of organic richness, hydrogen richness, kerogen type, maturity, and basin evolution, rather than reliance on a single parameter [1–3]. These studies provide a broad methodological framework for evaluating source rocks in both conventional and unconventional petroleum systems.

Within this broader context, deep and highly mature coal-measure source rocks have become increasingly important exploration targets in many petroliferous basins [4–7]. The Ordos Basin, one of the most important petroliferous basins in China, is a cratonic basin characterized by the superposition of multiple tectonic units [8,9]. The Upper Paleozoic Carboniferous–Permian coal-measure source rocks in the basin contain abundant natural gas resources and constitute the principal hydrocarbon source for major producing areas such as the Changqing Oilfield, thus carrying major strategic significance for the sustainable development of China's petroleum industry [10,11]. Studies in the Hangjinqi exploration area indicate that the Upper Paleozoic coal-bearing source rocks are characterized by very high organic matter abundance, with total organic carbon in coal seams reaching up to 61.32%, and relatively high thermal maturity, with R_o values of approximately 0.8%–1.3%, indicating entry into the peak gas-generation stage. These source rocks are dominated by Type III kerogen, and the total gas-generation capacity of the Shanxi Formation is significantly greater than that of the Taiyuan Formation [12]. Studies from the Ganquan area likewise show that multiple sets of source rocks are developed in the Upper Paleozoic, among which the source rocks of the Shanxi Formation are markedly superior to those of the Benxi Formation in both organic matter abundance and thickness, with source-rock thicknesses of 50–80 m. Overall, these rocks are at a high- to overmature stage and exhibit the characteristics of high-quality source rocks [13]. Collectively, these studies demonstrate that the Upper Paleozoic coal-measure source rocks are the principal source of natural gas in the Ordos Basin.

Despite the substantial achievements of the above regional studies, knowledge of the deep (>4000 m) source rocks in the Qingyang Gas Field of the Ordos Basin remains inadequate. A large deep coal-derived gas field sourced from highly thermally evolved thin coal seams has been discovered in the deep Qingyang Gas Field [14], with gas-bearing intervals occurring in the Taiyuan Formation, Shanxi Formation, and the He 8 Member of the Shihezi Formation. However, the geochemical characteristics of the deeply buried Shanxi–Taiyuan source rocks in the Qingyang Gas Field remain insufficiently constrained. In particular, for these source rocks buried at depths greater than 4000 m, their organic matter abundance, kerogen type, thermal maturity, and hydrocarbon-generation potential have not yet been systematically evaluated based on an integrated geochemical dataset.

This uncertainty limits a reliable assessment of their role in the Upper Paleozoic natural gas system.

In this study, mudstone source rocks from the Shanxi and Taiyuan Formations at depths of 4000–5000 m in the Qingyang Gas Field were selected as the research target. Integrated organic geochemical analyses, including TOC, Rock-Eval pyrolysis, chloroform bitumen "A", kerogen maceral composition, and vitrinite reflectance, were conducted in combination with natural gas composition, carbon isotope, formation water, and clay mineral data. The objectives of this study are to (1) characterize the organic matter abundance, type, and maturity of the deep Shanxi–Taiyuan source rocks; (2) examine the implications of natural gas geochemistry, formation water, and clay minerals for thermal evolution, preservation conditions, and diagenetic background; and (3) comprehensively evaluate the hydrocarbon-generation potential and heterogeneity of the source rocks. The results not only fill a major gap in the geochemical study of deep source rocks in the Qingyang Gas Field, but also provide regional case-study support for advancing hydrocarbon-generation theory for transitional marine–continental coal-measure source rocks. In addition, they provide fundamental geochemical constraints for further integrated exploration and evaluation in the study area and carry important theoretical value and practical significance for the exploration and development of analogous deep gas reservoirs.

2. Regional Geological Setting

The Ordos Basin, located in the western part of the North China Craton, is a large multicycle superimposed basin [15,16]. In plan view, it is expressed as a northwest–southeast-trending rectangular composite syncline and is subdivided into several second-order structural units, including the Yimeng Uplift, Western Shanxi Flexural Fold Belt, Yishan Slope, Western Margin Thrust Belt, Tianhuan Depression, and Weibei Uplift [17–20]. The Yishan Slope is an area of active hydrocarbon generation for Upper Paleozoic source rocks [21]. The Qingyang Gas Field is situated at the southern end of the southwestern Yishan Slope, within the transitional zone between the Weibei Uplift and the Tianhuan Depression, and lies in a triangular area bounded by the tectonically active Weibei Uplift and Western Margin Thrust Belt (Figure 1). Structurally, the study area is characterized by a broad, gentle west-dipping monocline with a gradient of approximately 6–10 m/km and bedding dips of less than 1°. Locally, NE-trending, low-amplitude, nose-like uplifts are developed, with amplitudes of about 10 m and widths of 4–5 km [14].

The Upper Paleozoic strata in the study area are relatively complete and, from bottom to top, mainly comprise the Carboniferous Taiyuan Formation and the Permian Shanxi and Shihezi formations (Figure 1). Owing to the influence of the Central Paleo-Uplift, the Benxi Formation is entirely absent in the study area, and the Taiyuan Formation is in direct contact with the Shanxi Formation. The Taiyuan Formation is approximately 120–180 m thick [22] and is composed mainly of dark mudstone, carbonaceous mudstone, coal seams, and bioclastic limestone. It represents tidal-flat to lagoonal deposition in a transitional marine–continental setting and constitutes an important coal-measure source-rock interval. The Shanxi Formation is approximately 80–130 m thick and can be subdivided into the Shan 2 and Shan 1 members. The Shan 2 Member contains coal seams, carbonaceous mudstone, and dark mudstone and forms the principal source-rock interval, whereas sandstone bodies are well developed in the Shan 1 Member, which was deposited in delta-plain to swamp environments. Together, the Shanxi and Taiyuan Formations constitute the core source-rock succession of the Upper Paleozoic natural gas system in the Ordos Basin. The associated coal-measure source rocks are characterized by either self-sourcing and self-storage or lower-source/upper-reservoir accumulation styles.

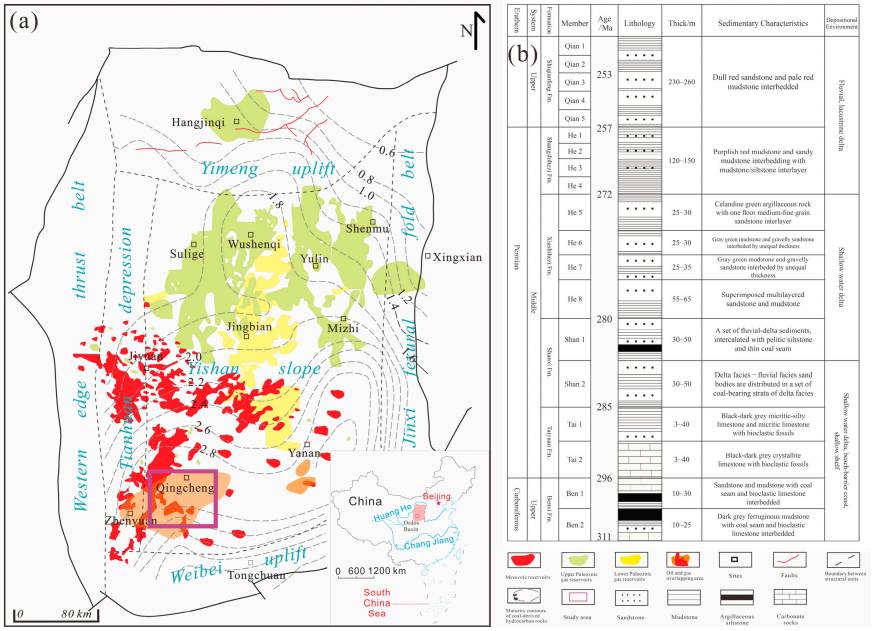


Figure 1. (**a**) Structural location diagram and (**b**) composite stratigraphic column of the study area. The inset map of China is adapted from the standard map available on the Standard Map Service website of the National Administration of Surveying, Mapping and Geoinformation of China (http://bzdt.ch.mnr.gov.cn/ (accessed on 26 April 2026), GS(2016)1549).

Under the influence of the Central Paleo-Uplift, the Upper Paleozoic succession in the study area is relatively thin and is noticeably thinner than in the central and eastern parts of the basin, forming an evolutionary pattern characterized by thin sedimentary successions, great burial depths, and weak erosion. As a result, the Shanxi–Taiyuan source rocks are generally buried at depths greater than 4000 m and occur under high-temperature and high-pressure conditions, which provided sufficient thermal energy for organic matter maturation and natural gas generation. The stable tectonic background of the Ordos Basin, the Late Paleozoic transitional marine–continental to continental depositional framework, and the favorable tectono-sedimentary setting of the Yishan Slope together controlled the development and distribution of the thick, high-quality coal-measure source rocks of the Shanxi and Taiyuan Formations.

3. Sample Collection and Analytical Methods

3.1. Sample Collection and Selection

The materials analyzed in this study include mudstone samples, natural gas samples, and formation-water samples. A total of 20 mudstone samples were collected from the Shanxi and Taiyuan Formations at depths of 4000–5000 m. These samples cover the major available sampling wells, stratigraphic intervals, and burial-depth ranges in the study area. All 20 samples were used for clay mineral analysis. Among them, 13 samples were selected for TOC, Rock-Eval pyrolysis, chloroform bitumen "A", kerogen maceral composition, and vitrinite reflectance analyses. The selection of these 13 samples was mainly based on lithological representativeness, stratigraphic coverage, sample freshness, absence of obvious drilling-mud contamination or weathering, and sufficient sample mass for multiple organic geochemical analyses. During data checking, however, Sample 3 was found to have unreliable organic geochemical data, most likely due to contamination during sampling or preparation; therefore, it was excluded from the statistical evaluation and subsequent interpretation of the TOC and Rock-Eval dataset. The remaining seven mudstone samples were not subjected to the full suite of organic geochemical tests because of limited sample

mass or because they were primarily used to improve the depth coverage of clay mineral analysis. This selection strategy ensured that the organic geochemical sample subset was representative of the major source-rock intervals, while also providing sufficient material for reliable analytical procedures. The sample information is listed in Table 1. In addition, eight natural gas samples were collected (Table 2), together with ten formation-water samples (Table 3).

Table 1. Analysis of mudstone sample: test statistics.

No.	Well No.	Formation	Depth (m)	Rock-Eval Pyrolysis	Chloroform Bitumen "A"	Kerogen Composition	Vitrinite Reflectance	Clay Minerals
1	L48	Shanxi Formation	4117.30	1	1	1	1	1
2	L48	Shanxi Formation	4116.35					1
3	L48	Shanxi Formation	4115.14	1	1	1	1	1
4	L65	Shanxi Formation	4243.84	1	1	1	1	1
5	L65	Shanxi Formation	4242.85	1	1	1	1	1
6	L65	Shanxi Formation	4221.90					1
7	L59	Shanxi Formation	4790.90	1	1	1	1	1
8	L59	Shanxi Formation	4789.80	1	1	1	1	1
9	L59	Shanxi Formation	4788.95					1
10	L59	Shanxi Formation	4775.80	1	1	1	1	1
11	L67	Taiyuan Formation	4415.65					1
12	L67	Taiyuan Formation	4414.50	1	1	1	1	1
13	L67	Taiyuan Formation	4413.75					1
14	HT2	Taiyuan Formation	4606.72	1	1	1	1	1
15	HT2	Taiyuan Formation	4604.65					1
16	HT2	Taiyuan Formation	4603.09	1	1	1	1	1
17	L64	Taiyuan Formation	4519.23	1	1	1	1	1
18	L64	Taiyuan Formation	4517.99					1
19	L64	Taiyuan Formation	4516.00	1	1	1	1	1
20	L64	Taiyuan Formation	4515.08	1	1	1	1	1

Table 2. Analysis of natural gas sample: test statistics.

No.	Well No.	Formation	Top Depth (m)	Base Depth (m)	Natural Gas Composition	Carbon Isotopic Composition of Natural Gas
1	L1	Shanxi Formation	4256	4276	1	1
2	QT3	Shanxi Formation	4247	4251	1	1
3	ZT1	Shanxi Formation	4393	4396	1	1
4	ZT1	Shanxi Formation	4493	4496	1	1
5	L67	Taiyuan Formation	4419	4428	1	1
6	L68	Taiyuan Formation	4492	4496	1	1
7	L77	Taiyuan Formation	4751	4756	1	1
8	L98	Taiyuan Formation	4462	4470	1	1

Table 3. Analysis of formation water sample: test statistics.

No.	Well No.	Formation	Top Depth (m)	Base Depth (m)	Formation Water Analysis
1	QT1	Shanxi Formation	4281	4284	1
2	QT4	Shanxi Formation	4377	4380	1
3	QT4	Shanxi Formation	4317	4380	1
4	L65	Shanxi Formation	4208	4210	1
5	L60	Shanxi Formation	4449	4464.5	1
6	L55	Taiyuan Formation	4004	4006	1
7	L67	Taiyuan Formation	4419	4428	1
8	L68	Taiyuan Formation	4492	4496	1
9	L77	Taiyuan Formation	4751	4756	1
10	L98	Taiyuan Formation	4462	4470	1

3.2. Organic Geochemical Analyses of Mudstone Samples

The analytical procedures applied to the mudstone samples are as follows:

(1) Total organic carbon (TOC) content was determined for 13 representative mudstone samples. The samples were first crushed into fine powder with a grain size of less than 0.2 mm and then treated with hydrochloric acid to remove carbonate minerals. After decalcification, the residual samples were repeatedly rinsed with deionized water to neutral pH and dried at low temperature. TOC contents were subsequently measured using a LECO CS-230 carbon–sulfur analyzer (LECO Corporation, St. Joseph, MI, USA), following the Chinese national standard GB/T 19145-2022 Determination of Total Organic Carbon in Sedimentary Rocks [23]. Prior to analysis, the instrument was calibrated using certified reference materials, and analytical blanks and replicate samples were included for quality control. Based on repeated analyses of standard and duplicate samples, the analytical precision was generally better than ±5%.

(2) Rock-Eval pyrolysis was conducted to evaluate the residual hydrocarbon-generation potential of the source rocks. Thirteen representative mudstone samples were analyzed using a Rock-Eval 6 pyrolyzer (Vinci Technologies, Nanterre, France) following the Chinese national standard GB/T 18602-2012 [24], Rock Pyrolysis Analysis. Before analysis, weathered surfaces and possible drilling-mud contamination were removed, and the samples were crushed and homogenized to a particle size of less than 150 mesh. Approximately 60 mg of powdered sample was weighed for each analysis. The pyrolysis experiment was carried out under an inert atmosphere using high-purity nitrogen as the carrier gas. Free hydrocarbons, expressed as S1, were released by holding the sample at 300 °C for 3 min. The remaining hydrocarbon-generation potential, expressed as S2, was then obtained by programmed pyrolysis from 300 °C to 600 °C at a heating rate of 25 °C/min. Tmax was defined as the temperature corresponding to the maximum yield of the S2 peak, rather than the maximum experimental temperature. The hydrogen index (HI) and production index (PI) were calculated as HI = S2 × 100/TOC and PI = S1/(S1 + S2), respectively. Before sample analysis, the instrument was calibrated using laboratory reference materials, and analytical blanks were run regularly to monitor background signals. Selected samples were analyzed in duplicate to evaluate reproducibility. The analytical reproducibility of S1 and S2 was generally better than 5% relative standard deviation, and the uncertainty of Tmax was approximately ±2 °C. For samples with very low S2 values, especially S2 < 0.2 mg HC/g rock, Tmax and HI were interpreted cautiously because weak or broad S2 peaks may lead to unreliable maturity and kerogen-type indications.

(3) To determine the soluble organic matter content, namely chloroform bitumen "A", Soxhlet extraction was performed on the same 13 representative mudstone samples following the Chinese petroleum industry standard SY/T 5118-2021 [25], Determination of Extract Content in Rocks. Before extraction, weathered surfaces and possible drilling-mud contamination were removed, and the samples were crushed to 100–120 mesh and dried at 40 °C. Approximately 50 g of powdered sample was weighed using an analytical balance with a readability of 0.1 mg and then loaded into a cellulose filter-paper thimble. The samples were extracted with chromatographic-grade chloroform using a standard Soxhlet extraction apparatus for 72 h, with a reflux frequency of approximately 4–6 cycles per hour. After extraction, the solvent was removed using a rotary evaporator at temperatures below 40 °C, followed by nitrogen blowdown to near dryness. The extracted chloroform bitumen "A" was weighed using the same analytical balance, and its content was calculated relative to the original rock mass. Procedural blanks were included to monitor possible contamination from solvents and glassware. All solvents were chromatographic grade, and all glassware was thoroughly cleaned and dried before use. Selected samples were

extracted in duplicate to evaluate reproducibility, and the relative deviation of chloroform bitumen "A" yield was generally less than 5%.

(4) Kerogen maceral composition analysis was performed on the same 13 representative mudstone samples to determine the organic matter type. Kerogen was first isolated from the powdered rock samples by acid treatment to remove carbonate and silicate minerals. The separated kerogen residues were then mounted on glass slides and examined using a Zeiss Axio Scope A1 transmitted-light and fluorescence microscope (Carl Zeiss Microscopy GmbH, Jena, Germany), following the Chinese petroleum industry standard SY/T 5125-2014 [26], Method of Identification and Type Classification of Kerogen Macerals by Transmitted Light and Fluorescence. Sapropelinite, exinite, vitrinite, and inertinite were identified according to their optical characteristics under transmitted light and fluorescence. Where sufficient organic particles were available, at least 300 valid particles were counted for each sample, and the relative proportion of each maceral group was calculated. Duplicate counts were conducted for selected samples to evaluate reproducibility, and the relative deviation of the dominant maceral components was generally less than 10%.

(5) Vitrinite reflectance (R_o) was measured on polished blocks prepared from the same 13 representative mudstone samples to evaluate thermal maturity. Representative rock fragments were embedded in epoxy resin, ground successively with abrasive papers, polished with diamond suspension, and finally finished with alumina powder to obtain a smooth mirror-like surface. R_o measurements were conducted using an MPV-SP microspectrophotometer attached to a reflected-light microscope, following the Chinese petroleum industry standard SY/T 5124-2012 [27], Method for Determining Vitrinite Reflectance in Sedimentary Rocks. The measurements were performed under oil immersion using monochromatic light at 546 nm. The instrument was calibrated before analysis using certified reflectance standards. For each sample, more than 30 valid vitrinite particles were measured where possible, depending on the abundance and preservation of vitrinite particles. Clearly reworked, oxidized, bitumen-like, or anomalous particles were excluded. The reported R_o value represents the arithmetic mean of valid measurements. Repeat measurements of standards and selected samples indicate that the analytical uncertainty was generally within $\pm 0.05\%$ R_o.

3.3. Clay Mineral Analysis

X-ray diffraction (XRD) analysis of clay minerals was conducted on all 20 mudstone samples to determine clay mineral composition and relative abundance. The analysis was performed using a Rigaku D/Max-2500 X-ray diffractometer (Rigaku Corporation, Akishima-shi, Tokyo, Japan) following the Chinese petroleum industry standard SY/T 5163-2018 [28], Analysis Method for Clay Minerals and Common Non-Clay Minerals in Sedimentary Rocks by X-ray Diffraction. Prior to analysis, weathered surfaces and possible contaminants were removed, and the samples were crushed to fine powder. Organic matter was removed using hydrogen peroxide, and the clay-sized fraction (<2 μm) was separated by sedimentation and centrifugation. Oriented clay mounts were prepared on glass slides and analyzed under air-dried, ethylene-glycol-saturated, and 550 °C heated conditions to distinguish illite, kaolinite, chlorite, and illite/smectite mixed-layer minerals. XRD measurements were performed using Cu Kα radiation at 40 kV and 40 mA, with a scanning range of 3–30° 2θ, a step size of 0.02°, and a scanning speed of 2°/min. The relative contents of clay minerals were calculated from diagnostic peak areas using correction factors according to SY/T 5163-2018 [28]. Instrument stability was checked using standard reference materials before analysis, and selected samples were repeatedly scanned to evaluate reproducibility. The relative deviation of repeated measurements for major clay mineral components was generally less than 10%.

3.4. Natural-Gas and Formation-Water Analyses

A total of eight natural gas samples were collected from the Shanxi and Taiyuan Formations for gas-composition and carbon-isotope analyses. Natural gas composition was determined using an Agilent 6890N gas chromatograph (Agilent Technologies, Inc., Santa Clara, CA, USA) equipped with a thermal conductivity detector (TCD) and a flame ionization detector (FID), following the Chinese national standard GB/T 13610-2020 [29], Analysis of Natural Gas Composition—Gas Chromatography. Before analysis, the gas chromatograph was calibrated using certified natural-gas standard mixtures. The main hydrocarbon components, including CH_4, C_2H_6, C_3H_8, i-C_4H_{10}, n-C_4H_{10}, i-C_5H_{12}, and n-C_5H_{12}, as well as non-hydrocarbon gases such as N_2 and CO_2, were quantitatively determined. Component concentrations were calculated using external standard calibration and normalized to volume percentage. Analytical blanks and duplicate analyses were performed to monitor instrument stability and reproducibility. The relative standard deviation of repeated measurements for major gas components was generally less than 2%, whereas that for minor components was generally less than 5%.

Carbon isotope analysis of natural gas was performed on all eight gas samples using a Thermo Fisher Scientific MAT-253, gas isotope-ratio mass spectrometer (Thermo Fisher Scientific (Bremen) GmbH, Bremen, Germany), coupled to a gas chromatograph through a combustion interface, following the Chinese petroleum industry standard SY/T 5238-2019 [30], Analysis Method for Carbon and Oxygen Isotopes of Organic Matter and Carbonate. Individual hydrocarbon components were first separated by gas chromatography and then introduced into a high-temperature combustion interface, where they were quantitatively converted to CO_2 in the presence of an oxidation catalyst. The generated CO_2 was subsequently introduced into the isotope ratio mass spectrometer for carbon isotope analysis. The carbon isotope compositions are reported in δ notation relative to the Vienna Pee Dee Belemnite standard (VPDB). Reference CO_2 gas and certified isotope standards were used for calibration before and during analysis. Duplicate analyses were conducted for selected samples, and the analytical precision of $\delta^{13}C$ measurements was generally better than $\pm 0.3‰$.

In addition, ten formation-water samples were collected from the Shanxi and Taiyuan Formations for hydrochemical analysis. The concentrations of major cations and anions were determined following the Chinese petroleum industry standard SY/T 5523-2016 [31], Method for Analysis of Oilfield Water. Na^+ and K^+ were measured by flame photometry or ion chromatography, Ca^{2+} and Mg^{2+} by titration or inductively coupled plasma optical emission spectrometry, and Cl^-, SO_4^{2-}, and HCO_3^- by ion chromatography or titration according to the laboratory procedure. Total dissolved solids (TDS) were calculated from the measured ionic concentrations, and hydrochemical facies were classified using the Sulin classification method. Calibration was performed using standard solutions, and analytical blanks and duplicate samples were included for quality control. The reliability of the water-chemistry data was evaluated using ionic charge-balance error, which was generally within ±5%.

4. Results and Discussion

4.1. Organic Geochemical Characteristics of the Source Rocks

Detailed TOC, Rock-Eval pyrolysis parameters, calculated geochemical indices, and vitrinite reflectance data for the representative mudstone samples are summarized in Table 4. Although 13 mudstone samples were initially selected for Rock-Eval pyrolysis analysis, the Rock-Eval parameters of Sample 3 were considered unreliable, most likely due to contamination during sampling or sample preparation, and were therefore excluded from the statistical evaluation and subsequent interpretation. Consequently, the Rock-Eval-based

evaluation was conducted using the remaining 12 valid samples. The measured parameters include TOC, S1, S2, Tmax, and vitrinite reflectance, whereas the calculated indices include S1 + S2, HI, and PI. Together, these parameters provide the basis for evaluating organic matter abundance, organic matter type, and thermal maturity at the sample scale.

Table 4. TOC contents, Rock-Eval pyrolysis parameters, calculated geochemical indices, and vitrinite reflectance data of mudstone samples from the Shanxi and Taiyuan Formations.

No.	Well No.	Formation	Depth (m)	TOC (wt.%)	S1 (mg/g)	S2 (mg/g)	Tmax (°C)	S1 + S2 (mg/g)	HI (mg/g TOC)	PI	R_o (%)
1	L48	Shanxi Formation	4117.30	0.70	0.6269	6.2797	440	6.9066	897.1000	0.0908	2.03
3	L48	Shanxi Formation	4115.14	/	/	/	/	/	/	/	/
4	L65	Shanxi Formation	4243.84	0.89	0.5705	2.8628	447	3.4333	321.6629	0.1662	2.04
5	L65	Shanxi Formation	4242.85	2.53	0.0468	0.1506	438	0.1974	5.9526	0.2371	2.04
7	L59	Shanxi Formation	4790.90	0.07	0.0438	0.1432	475	0.1870	204.5714	0.2342	2.22
8	L59	Shanxi Formation	4789.80	1.33	0.8794	5.5890	462	6.4684	420.2256	0.1360	2.21
10	L59	Shanxi Formation	4775.80	0.09	0.0456	0.1229	465	0.1685	136.5556	0.2706	2.18
12	L67	Taiyuan Formation	4414.50	0.60	0.0267	0.0681	436	0.0948	11.3500	0.2816	2.07
14	HT2	Taiyuan Formation	4606.72	0.38	0.0488	0.1061	472	0.1549	27.9211	0.3150	2.17
16	HT2	Taiyuan Formation	4603.09	0.88	0.1109	0.2409	482	0.3518	27.3750	0.3152	2.14
17	L64	Taiyuan Formation	4519.23	1.52	0.6841	3.3572	482	4.0413	220.8684	0.1693	2.13
19	L64	Taiyuan Formation	4516.00	0.11	0.0447	0.1301	442	0.1748	118.2727	0.2557	2.07
20	L64	Taiyuan Formation	4515.08	0.19	0.0319	0.0890	420	0.1209	46.8421	0.2639	2.07

Note: TOC = total organic carbon; S1 = free hydrocarbons; S2 = remaining hydrocarbon-generation potential; Tmax = temperature of maximum S2 generation; HI = hydrogen index; PI = production index; R_o = mean vitrinite reflectance. HI = S2 × 100/TOC; PI = S1/ (S1 + S2). Sample 3 was excluded from the statistical evaluation and subsequent interpretation because its Rock-Eval parameters were considered unreliable, most likely due to contamination during sampling or preparation.

4.1.1. Organic Matter Abundance

Organic matter abundance is a fundamental parameter for evaluating the material basis of hydrocarbon generation in source rocks. Commonly used indicators include total organic carbon (TOC), chloroform bitumen "A", and Rock-Eval pyrolysis parameters, including S1, S2, and total hydrocarbon-generating potential (S1 + S2). The classification and evaluation of these parameters can be carried out in accordance with the petroleum and natural gas industry standard Geochemical Evaluation Methods for Source Rocks (SY/T 5735–2019) [32]. Similar integrated organic geochemical approaches have been widely applied in source-rock evaluation studies from different petroliferous basins, in which TOC, Rock-Eval pyrolysis parameters, extractable organic matter, kerogen type, and maturity indicators are jointly used to evaluate organic matter abundance, quality, and hydrocarbon-generation potential [33–36].

In this study, TOC is used mainly as an indicator of organic matter abundance, but it is not interpreted alone as a measure of source-rock effectiveness. Hydrocarbon generation also depends on the hydrogen richness, kerogen type, and thermal maturity of the organic matter [37]. Therefore, TOC is interpreted together with hydrogen-related Rock-Eval parameters, especially S2, S1 + S2, and HI, as well as kerogen maceral composition and maturity indicators [38]. For the high- to overmature samples analyzed in this study, S2, HI, and S1 + S2 mainly record the amount of residual pyrolyzable organic matter and residual Rock-Eval hydrocarbon-generating capacity after hydrocarbon generation, expulsion, and thermal cracking. These parameters are therefore used primarily to compare the relative quality and heterogeneity of the sampled intervals.

The TOC contents of the 12 valid mudstone samples from the Shanxi and Taiyuan Formations range from 0.07% to 2.53%, with an average of 0.77% (Table 4). Based on the commonly used TOC classification criteria for Type II_2–III continental to transitional source rocks—non-source rock, <0.5%; poor, 0.5%–1.0%; fair, 1.0%–2.5%; good, 2.5%–4.0%; and excellent, >4.0% [37,38]—the organic matter abundance of these mudstone source rocks is generally evaluated as poor to fair. Only a few samples reach the fair category,

among which Sample 5 has a TOC value of 2.53%, reaching the lower limit of the good category. These results indicate pronounced heterogeneity in organic matter enrichment, suggesting that relatively better source-rock intervals are developed only locally within specific stratigraphic intervals or sedimentary facies belts.

Chloroform bitumen "A" contents range from 0.0018% to 0.0147%, with an average of 0.006%. According to SY/T 5735–2019 [32], samples with chloroform bitumen "A" contents lower than 0.015% fall within the very low to low categories, indicating that the samples from the study area are generally depleted in soluble organic matter under the present high- to overmature conditions. The relationship between chloroform bitumen "A" and TOC is shown in Figure 2a. All samples show relatively low chloroform bitumen "A" contents, and no obvious positive correlation with TOC is observed. In particular, some samples with relatively high TOC contents still show low chloroform bitumen "A" contents, indicating that soluble organic matter abundance is not completely controlled by total organic carbon content. This feature may reflect not only relatively low initial organic matter abundance, but also the depletion of soluble organic components during deep burial as a result of hydrocarbon expulsion and thermal cracking. As also shown in Figure 2a, the hydrocarbon-generating capacity of the Shanxi and Taiyuan Formation mudstones is generally poor to fair, with some local samples tending toward better-quality source rocks.

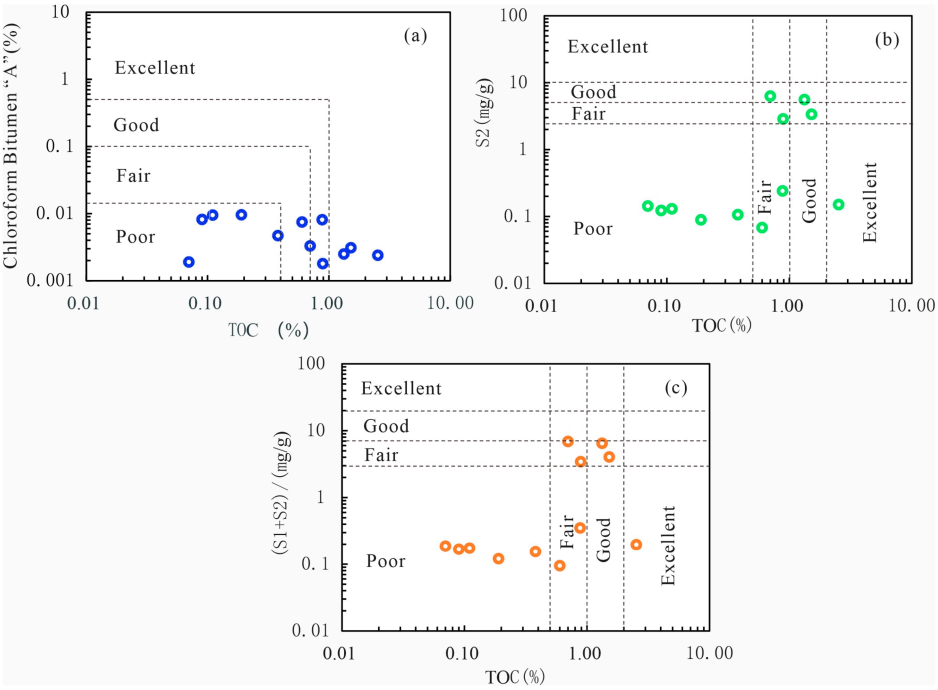


Figure 2. Hydrocarbon generation potential of source rocks in the Shanxi and Taiyuan Formations, Qingyang Gas Field. (**a**) Relationship between chloroform bitumen "A" and TOC; (**b**) relationship between S2 and TOC; (**c**) relationship between S1 + S2 and TOC.

Rock-Eval results show that S2 values of the 12 valid samples range from 0.0681 to 6.2797 mg/g, with an average of 1.5946 mg/g, whereas S1 + S2 values range from 0.0948 to 6.9066 mg/g, with an average of 1.8582 mg/g (Table 4). These values indicate that the residual hydrocarbon-generating capacity of the studied samples is generally limited. Most samples have relatively low S2 and S1 + S2 values, whereas only a few samples, especially Samples 1, 8, and 17, show relatively high S2 and S1 + S2 values.

The TOC–S2 cross-plot reveals the relationship between organic matter abundance and hydrogen-related pyrolyzable organic matter (Figure 2b). TOC reflects organic carbon content, whereas S2 represents hydrocarbons generated from pyrolyzable organic matter

during Rock-Eval analysis. Therefore, the combined use of TOC and S2 provides a more reliable evaluation of source-rock effectiveness than TOC alone. In Figure 2b, most samples plot within the poor to fair fields of residual hydrocarbon-generating capacity, whereas only a few samples tend toward the good field.

The relationship between S1 + S2 and TOC shows that samples with relatively high organic matter abundance do not always have proportionally higher Rock-Eval hydrocarbon-generating capacity (Figure 2c). For example, Sample 5 has the highest TOC value of 2.53%, but its S2 and S1 + S2 values are only 0.1506 and 0.1974 mg/g, respectively. In contrast, Samples 1 and 8 have lower TOC values of 0.70% and 1.33%, respectively, but their S2 values are significantly higher, at 6.2797 and 5.5890 mg/g, respectively. These contrasts indicate that TOC alone cannot reliably characterize source-rock effectiveness and that the abundance of hydrogen-rich and pyrolyzable components in the organic matter must also be considered.

In summary, TOC, chloroform bitumen "A", S1 + S2, and S2 provide complementary constraints on organic matter abundance and residual hydrocarbon-generating capacity from different perspectives. TOC values indicate that the organic matter abundance of the Shanxi and Taiyuan Formation mudstones is generally poor to fair, with locally developed organic-rich intervals. Chloroform bitumen "A" contents are generally low, indicating limited residual soluble organic matter under the present high- to overmature conditions. Rock-Eval S1 + S2 and S2 values further indicate that most samples contain limited residual pyrolyzable organic matter, whereas only a few samples, such as Samples 1, 8, and 17, show relatively better Rock-Eval responses. The contrast between Sample 5, which has the highest TOC but a very low S2 value, and Samples 1 and 8, which have lower TOC but significantly higher S2 values, demonstrates that TOC alone cannot fully characterize source-rock effectiveness. Therefore, the source rocks in the study area are interpreted to have generally poor to fair organic matter abundance and residual hydrocarbon-generating capacity, with relatively better intervals developed locally.

4.1.2. Organic Matter Type

Organic matter type is a key control on the hydrocarbon-generation pathways of source rocks and can be determined through integrated analysis of kerogen maceral composition (e.g., sapropelinite, exinite, and inertinite) and Rock-Eval parameters, such as HI, OI, or HI constrained by S_2–TOC regression [39–41]. It should be noted, however, that in mature to overmature samples, HI and OI tend to converge toward lower values with progressive thermal evolution [42,43]. Therefore, identifying the original kerogen type solely on the basis of HI or HI–Tmax may introduce systematic bias [44,45]. Accordingly, this study primarily relies on maceral composition, with pyrolysis parameters used as supporting evidence.

Microscopic identification of kerogen macerals shows that sapropelinite accounts for 9.64%–73% of the kerogen in the mudstone samples from the study area, exinite comprises 0.1%–4.11%, and inertinite 0.8%–5.91%. Kerogen Types I, II_1, II_2, and III are all present. Rock-Eval results indicate HI values ranging from 5.9526 to 897.1000 mg/g TOC, with an average of 203.2248 mg/g TOC. Because HI is calculated as (S2 × 100)/TOC, it may be artificially inflated in samples with low TOC, and its type-indicative significance may also be affected by matrix adsorption as well as contamination or bitumen-related effects. Therefore, the S2–TOC plot (following the Langford and Blanc-Valleron method) was used to further evaluate matrix effects and constrain the true HI.

On the HI–Tmax diagram, most samples plot within or close to the Type III field, whereas several samples fall toward the Type II or Type I fields (Figure 3). This distribution should not be interpreted as indicating discrete single kerogen types for individual samples.

Instead, it reflects a kerogen mixing effect caused by variable proportions of humic and sapropelitic organic matter in the transitional marine–continental depositional setting. Previous studies have shown that mixed kerogen types are common in sedimentary source rocks and that Rock-Eval-based kerogen classification may be affected by kerogen mixing, mineral matrix effects, and thermal maturity [38,46].

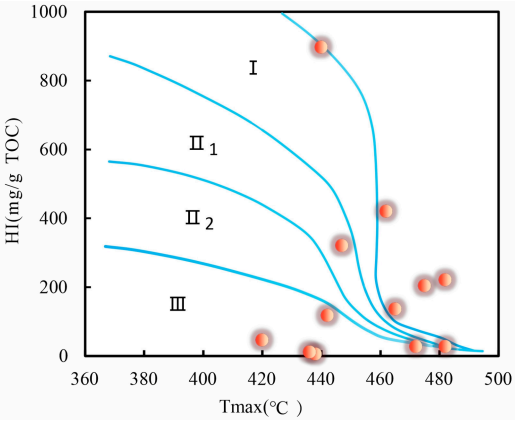


Figure 3. Organic matter types of source rocks in the Shanxi and Taiyuan Formations, Qingyang Gas Field. (I) Sapropelic; (II_1) humic-sapropelic; (II_2) sapropelic-humic; (III) humic.

In the present study, microscopic maceral observations indicate the coexistence of sapropelinite, exinite, vitrinite, and inertinite, supporting a mixed organic-matter assemblage rather than a single kerogen end-member. The relatively high proportion of humic components indicates that the source rocks are generally dominated by Type III kerogen and have an overall gas-prone character. However, locally higher sapropelinite contents and relatively high HI values in some samples suggest subordinate oil- or condensate-prone components. Because the samples are high to overmature and some low-TOC samples may show unstable or artificially elevated HI values, the HI–Tmax diagram is used only as supporting evidence. Therefore, the organic matter type is interpreted as Type III-dominated mixed kerogen, with subordinate Type II and minor Type I components in some samples.

4.1.3. Thermal Maturity of Organic Matter

Thermal maturity of organic matter is used to evaluate whether source rocks have entered the hydrocarbon-generation window and to constrain their stage of thermal evolution. However, the interpretation of maturity stages should take into account the dominant organic matter type, because oil-prone and gas-prone kerogens may enter hydrocarbon-generation stages at different R_o thresholds. Dembicki Jr. emphasized that vitrinite reflectance should not be interpreted independently of kerogen type and geological context. For gas-prone organic matter, R_o values of <0.8%, 0.8%–1.2%, 1.2%–2.0%, and >2.0% generally correspond to immature, early gas-generation, peak gas-generation, and late gas-generation to dry-gas stages, respectively [46].

In this study, thermal maturity was evaluated comprehensively using vitrinite reflectance (R_o), maximum pyrolysis temperature (Tmax), and natural gas carbon-isotope characteristics. Because the organic matter in the Shanxi and Taiyuan Formation source rocks is interpreted as Type III-dominated mixed kerogen with an overall gas-prone character, the maturity interpretation was adjusted using a gas-prone generation framework rather than a single general R_o scale. Vitrinite reflectance results show that R_o values of the source rocks range from 2.03% to 2.22%, with an average of 2.11%, indicating that the source rocks have generally reached the peak to late gas-generation stage (Figure 4a). Therefore, the studied source rocks are interpreted as high to overmature, with maturity conditions favorable for dry gas generation from Type III-dominated organic matter.

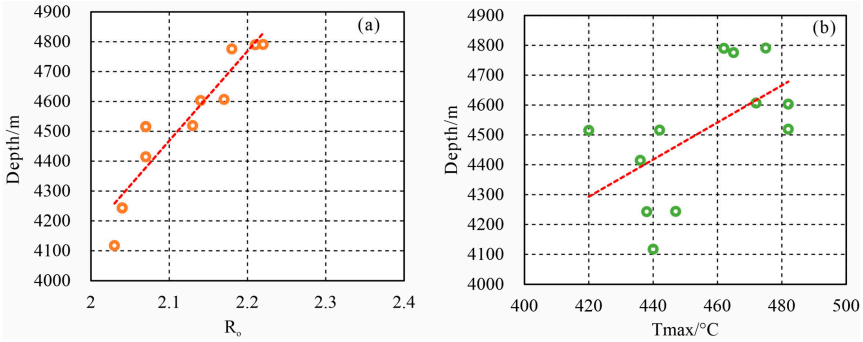


Figure 4. Relationships of (**a**) vitrinite reflectance (R_o) and (**b**) Tmax with burial depth for source rocks of the Shanxi and Taiyuan Formations in the Qingyang Gas Field.

Measured Tmax values of the valid Rock-Eval samples range from 420 to 482 °C (Figure 4b). However, Tmax should be interpreted cautiously because several samples have very low S2 values and weak pyrolysis peaks, which may reduce the reliability of Tmax. Therefore, R_o is used as the primary maturity indicator in this study, whereas Tmax is used only as a supplementary parameter.

The carbon isotopic compositions of natural gas show that $\delta^{13}C_1$ values range from −35.59‰ to −20.65‰, with an average of −29.82‰, whereas $\delta^{13}C_2$ values range from −37.82‰ to −28.44‰, with an average of −33.78‰. Overall, the gases exhibit an isotopic reversal characterized by $\delta^{13}C_1 > \delta^{13}C_2$, which is a typical feature of cracking gas derived from humic organic matter at the high- to overmature stage. This further corroborates the advanced thermal evolution of the mudstone source rocks.

4.2. Conditions Favorable for Hydrocarbon Generation

4.2.1. Geochemical Characteristics of Formation Water

The geochemical characteristics of subsurface water exert an important influence on the preservation and transformation of organic matter, as well as on hydrocarbon migration and accumulation [47–50]. Analytical results for formation water samples from the study area show that total dissolved solids range from 6.59 to 61.15 g/L, with an average of 25.56 g/L, indicating medium- to high-salinity formation water. Formation waters of moderate to high salinity generally suggest weak exchange with external meteoric freshwater and a relatively closed hydrologic system, conditions that favor the development of relatively reducing and stabilizing preservation environments and thus enhance the likelihood of hydrocarbon preservation.

The results further indicate that the dominant hydrochemical facies is $CaCl_2$-type water. $CaCl_2$-type formation water typically develops in depositional systems with good sealing conditions and is conducive to the preservation of organic matter. At the same time, highly saline reducing environments can suppress oxidative decomposition of organic matter and promote kerogen degradation during thermal evolution, thereby favoring hydrocarbon generation. In addition, the relatively high HCO_3^- content in the formation water may be related to water–rock reactions involving organic acids and/or CO_2 generated during organic matter maturation and hydrocarbon generation [51,52].

4.2.2. Geochemical Characteristics of Natural Gas

Natural gas compositional data indicate (Figure 5a) that methane (C_1) contents in the study area range from 87.98% to 93.14%, with an average of 91.73%, whereas heavy hydrocarbons (C_2^+) range from 0.05% to 0.40%, averaging 0.16%, indicating a typical dry-gas composition. Among the nonhydrocarbon gases, N_2 contents range from 3.24% to 7.88%, with an average of 5.1%, and CO_2 contents range from 1.03% to 3.42%, with

an average of 1.93%. These results suggest that the natural gas experienced only weak meteoric water flushing during migration and has been well preserved. This characteristic is highly consistent with the carbon isotopic distribution pattern of hydrocarbons generated by thermal evolution of Type III kerogen: methane derived from humic organic matter generally exhibits relatively heavy carbon isotopic compositions, and the carbon isotopes of alkane gases become progressively enriched in ^{13}C with increasing thermal maturity.

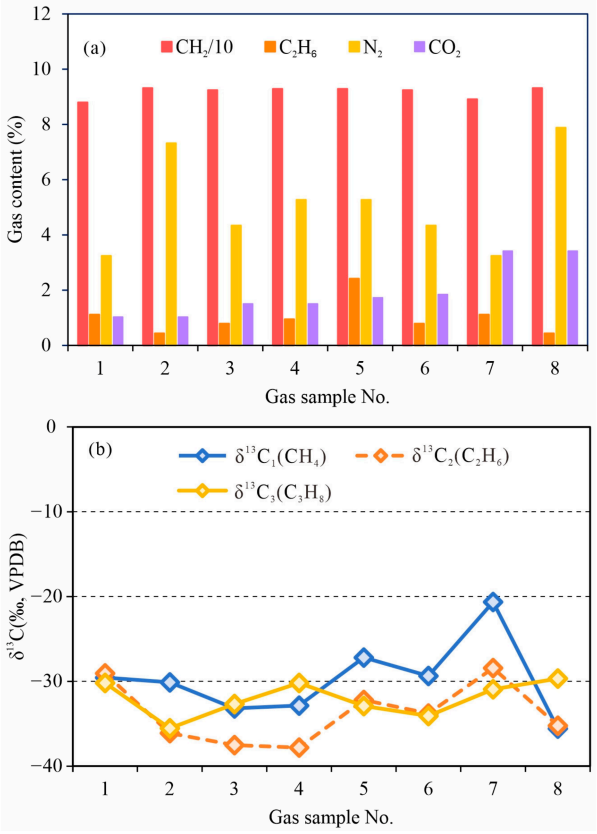


Figure 5. Natural gas composition and online carbon isotope analysis results. (**a**) Molecular composition of natural gas samples in which methane contents are plotted at one-tenth of their measured values for display. (**b**) Carbon isotope compositions of methane, ethane, and propane.

Online carbon isotope analysis of the natural gas shows (Figure 5b) that methane carbon isotopic values ($\delta^{13}C_1$) range from −35.59‰ to −20.65‰, whereas ethane carbon isotopic values ($\delta^{13}C_2$) range from −37.82‰ to −28.44‰. The overall combination of relatively heavy methane carbon isotopes and high gas dryness is a typical signature of high- to overmature coal-derived gas. In addition, the generally low contents of nonhydrocarbon gases, together with the carbon isotopic characteristics, further indicate that the gas reservoir has not been significantly modified by meteoric freshwater flushing, mixing with shallow biogenic gas, or magmatic activity. The moderate N_2 contents were most likely derived from thermal decomposition of nitrogen-bearing organic matter in coal-measure source rocks, whereas the low CO_2 contents suggest only minor carbonate dissolution during reservoir formation. This, in turn, indicates that the strong sealing capacity of the mudstone aquitards provided favorable conditions for natural gas preservation.

4.2.3. Clay Mineral Characteristics and Their Implications for Diagenetic Conditions

Clay mineral assemblages can provide useful information on diagenetic conditions, fluid–rock interactions, and the preservation environment of deeply buried strata. In this study, X-ray diffraction (XRD) analysis was used to characterize the clay mineral composition of the Shanxi and Taiyuan Formation mudstones. The results (Figure 6)

indicate that, in the Shanxi Formation of the study area, illite content ranges from 11.37% to 37.58%, with an average of 27.46%; kaolinite ranges from 31.00% to 47.19%, averaging 41.82%; illite/smectite mixed-layer minerals range from 1.88% to 39.70%, with an average of 20.38%; and chlorite ranges from 3.30% to 20.12%, averaging 10.35%. In the Taiyuan Formation, illite content ranges from 6.25% to 62.00% (average 36.95%), kaolinite from 36.02% to 81.61% (average 49.64%), illite/smectite mixed-layer minerals from 0.57% to 14.34% (average 6.20%), and chlorite from 1.41% to 11.50% (average 7.21%). These values indicate that the reservoirs in the study area are in the transition from diagenetic Stage A to Stage B. The high kaolinite content suggests weakly acidic fluid activity during diagenesis, while the presence of chlorite reflects subsequent modification by weakly alkaline fluids.

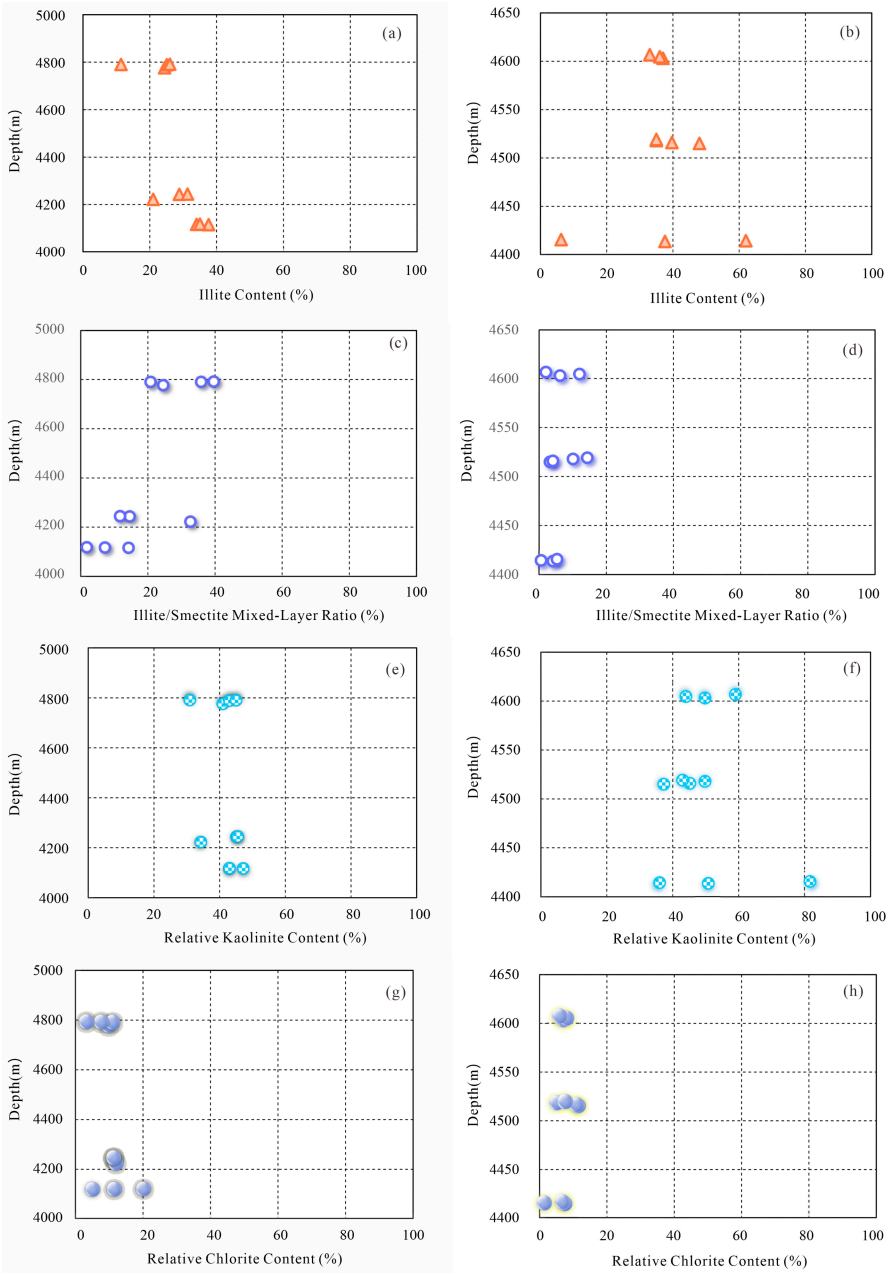


Figure 6. Clay mineral contents of source rocks from the Shanxi and Taiyuan Formations in relation to burial depth in the Qingyang Gas Field. (**a**,**c**,**e**,**g**) Samples from the Shanxi Formation; (**b**,**d**,**f**,**h**) samples from the Taiyuan Formation.

From the clay mineral variation with burial depth, both illite content and illite/smectite mixed-layer ratio show an overall increasing tendency in the deeper intervals (Figure 6a–d).

This trend is consistent with the progressive transformation of smectite to illite during burial diagenesis, which is commonly promoted by increasing burial temperature and thermal maturity. Therefore, the variation in illite and illite/smectite mixed-layer minerals indicates that the Shanxi–Taiyuan succession experienced burial-diagenetic modification. Kaolinite is an important clay mineral component in both the Shanxi and Taiyuan Formations and is dominant in many samples (Figure 6e,f). Its relatively wide compositional range suggests that kaolinite enrichment was controlled by both depositional conditions and diagenetic fluid–rock interaction. Acidic pore-fluid activity and feldspar dissolution during burial diagenesis may have promoted kaolinite formation, whereas differences between the Shanxi and Taiyuan Formations may also reflect variations in depositional facies and primary sediment supply. The chlorite contents show considerable sample-to-sample variation in both the Shanxi and Taiyuan Formations (Figure 6g,h). Based on the statistical results, the Shanxi Formation shows a slightly higher average chlorite content than the Taiyuan Formation. Combined with regional diagenetic context, this pattern suggests that the relatively mild diagenetic environment of the Shanxi Formation was more favorable for the primary preservation of chlorite, whereas the higher thermal evolution in the Taiyuan Formation led to partial mineral transformation or replacement by other minerals, reducing its abundance. In summary, the distribution patterns of clay minerals in the Shanxi–Taiyuan mudstones reflect the combined effects of depositional environment and diagenetic evolution.

4.3. Integrated Evaluation of Hydrocarbon-Generation Potential and Its Significance for Gas Accumulation

Based on integrated evidence from organic matter abundance, Rock-Eval pyrolysis parameters, kerogen maceral composition, thermal maturity, natural gas geochemistry, formation-water chemistry, and clay mineral assemblages, the Shanxi and Taiyuan Formation source rocks in the Qingyang Gas Field can be evaluated in terms of their Rock-Eval hydrocarbon-generating capacity and their geological significance for natural gas accumulation.

The TOC values of the 12 valid mudstone samples range from 0.07% to 2.53%, with an average of 0.77%, indicating generally poor to fair organic matter abundance. Rock-Eval results show that S2 values range from 0.0681 to 6.2797 mg/g, with an average of 1.5946 mg/g, whereas S1 + S2 values range from 0.0948 to 6.9066 mg/g, with an average of 1.8582 mg/g. These values indicate that the Rock-Eval hydrocarbon-generating capacity of the source rocks in the study area is generally limited. However, some samples, especially Samples 1, 8, and 17, show relatively high S2 and S1 + S2 values, suggesting that relatively better source-rock intervals are locally developed. Therefore, the Shanxi and Taiyuan Formation source rocks are generally characterized by poor to fair organic matter abundance and Rock-Eval hydrocarbon-generating capacity, with local improvement.

Organic matter type and maturity data further constrain the gas-generation significance of these source rocks. Kerogen maceral composition and Rock-Eval parameters indicate a Type III-dominated mixed kerogen assemblage, with subordinate Type II components and minor Type I components in some samples. This mixed organic-matter input reflects the transitional marine–continental depositional setting of the Shanxi and Taiyuan Formations, whereas the overall dominance of humic components indicates a mainly gas-prone source-rock system. Vitrinite reflectance values range from 2.03% to 2.22%, with an average of 2.11%, indicating that the source rocks have reached a high- to overmature stage. Although Tmax values range from 420 to 482 °C, Tmax is used only as a supplementary maturity indicator because several samples have low S2 values and weak pyrolysis peaks. Therefore, the maturity interpretation is mainly based on R_o values, together with natural gas geochemical evidence.

The natural gas geochemical data are consistent with the above source-rock interpretation. The natural gas is methane-rich, with an average methane content of 91.73%, whereas the average heavy hydrocarbon content is only 0.16%, indicating a typical dry-gas composition. The carbon isotope characteristics, including relatively heavy methane carbon isotope values and the observed isotope reversal, are consistent with high-maturity coal-derived gas generated from humic organic matter. These features indicate that, although the Rock-Eval hydrocarbon-generating capacity is generally limited, the Shanxi and Taiyuan Formation source rocks experienced effective natural gas generation during geological evolution and are genetically related to the present deep natural gas accumulation.

Formation-water chemistry and clay mineral assemblages provide further constraints on preservation conditions and diagenetic evolution. The medium- to high-salinity $CaCl_2$-type formation water indicates a relatively closed hydrologic environment favorable for natural gas preservation. The isotope reversal observed in the natural gas, together with its coal-derived gas affinity, supports a genetic link between hydrocarbon generation and present natural gas accumulation. In addition, the clay mineral assemblage dominated by kaolinite and illite, together with the evolutionary differences between the Shanxi and Taiyuan Formations, provides supporting evidence for understanding the diagenetic evolution, fluid–rock interaction, and preservation conditions of deeply buried strata.

Overall, the integrated geochemical evidence indicates that the Shanxi and Taiyuan Formation source rocks in the Qingyang Gas Field are heterogeneous. Their Rock-Eval hydrocarbon-generating capacity is generally poor to fair, but relatively better intervals are locally developed. The Type III-dominated mixed kerogen, high- to overmature R_o values, methane-rich dry-gas composition, and carbon isotope characteristics collectively indicate that these source rocks contributed to effective natural gas generation during geological evolution. Intervals where relatively better source-rock properties coincide with favorable reservoir, structural, and preservation conditions may have better exploration prospects, but this inference requires further validation using integrated geological, petrophysical, and production data.

5. Conclusions

The conclusions are as follows:

(1) The Shanxi and Taiyuan Formation source rocks in the Qingyang Gas Field are generally characterized by poor to fair organic matter abundance and limited Rock-Eval hydrocarbon-generating capacity, with local improvement. The TOC values of the 12 valid mudstone samples range from 0.07% to 2.53%, with an average of 0.77%. S2 values range from 0.0681 to 6.2797 mg/g, with an average of 1.5946 mg/g, whereas S1 + S2 values range from 0.0948 to 6.9066 mg/g, with an average of 1.8582 mg/g. These data indicate that the overall material basis for hydrocarbon generation is limited, although some samples show relatively better Rock-Eval responses.

(2) The organic matter is interpreted as a Type III-dominated mixed kerogen assemblage, with subordinate Type II components and minor Type I components in some samples, indicating mixed organic-matter input but an overall gas-prone character. Vitrinite reflectance values range from 2.03% to 2.22%, with an average of 2.11%, indicating that the source rocks have reached a high- to overmature stage. Tmax values range from 420 to 482 °C, but Tmax is used only as a supplementary maturity indicator because several samples have low S2 values and weak pyrolysis peaks. Therefore, thermal maturity is mainly constrained by R_o values and natural gas geochemical evidence.

(3) The formation-water, natural-gas, and clay-mineral data provide supplementary constraints on the preservation conditions, gas-generation significance, and diagenetic evolution of the Shanxi–Taiyuan source-rock system. Medium- to high-salinity $CaCl_2$-type

formation water indicates a relatively closed hydrologic environment, which is favorable for natural gas preservation. The natural gas is methane-rich, with an average methane content of 91.73% and an average heavy hydrocarbon content of only 0.16%, indicating a typical dry-gas composition. The carbon isotope characteristics, including relatively heavy methane carbon isotope values and isotope reversal, are consistent with high-maturity coal-derived gas generated from humic organic matter. Clay mineral assemblages dominated by kaolinite and illite reflect the combined influence of depositional conditions, burial diagenesis, and fluid–rock interaction.

(4) Overall, the integrated geochemical evidence indicates that the Shanxi and Taiyuan Formation source rocks are heterogeneous. Although their Rock-Eval hydrocarbon-generating capacity is generally limited, the Type III-dominated mixed kerogen, high- to overmature R_o values, methane-rich dry-gas composition, and carbon isotope characteristics collectively indicate that these source rocks experienced effective natural gas generation during geological evolution and are genetically related to the present deep natural gas accumulation. Locally improved source-rock intervals may have exploration significance where they coincide with favorable reservoir, structural, and preservation conditions, but this inference should be regarded as preliminary and requires further validation using spatial source-rock distribution, reservoir physical properties, gas-bearing characteristics, and production data.

Author Contributions: R.Y.: Conceptualization and Writing—original draft; C.Y.: Data Curation and Software and Writing—original draft; C.L.: Data Curation and Writing—original draft; Y.Z.: Investigation and Visualization; Y.D.: Investigation and Software; Y.K.: Data Curation; Z.C.: Methodology and Writing—review and editing. All authors have read and agreed to the published version of the manuscript.

Funding: This research was supported by the National Science and Technology Major Project, 2025ZD1010507, and the National Science and Technology Major Project, 2024ZD1403802.

Data Availability Statement: The original contributions presented in this study are included in the article. Further inquiries can be directed to the corresponding author.

Conflicts of Interest: Chao Ye, Chao Li, Yu Zhang, Yaxin Duan, and Yuanyuan Kou were employed by the Second Oil Production Plant, PetroChina Changqing Oilfield Company, Qingyang 745100, China. The paper reflects the views of the scientists and not the company.

References

1. Ahmed, A.; Jahandad, S.; Hakimi, M.H.; Gharib, A.F.; Mehmood, S.; Kahal, A.Y.; Khan, M.A.; Munir, M.N.; Lashin, A. Organic matter characteristics and conventional oil potentials of shales from the Early Jurassic Datta Formation in the Upper Indus Basin, Northern Pakistan. *J. Asian Earth Sci.* **2022**, *224*, 104975. [CrossRef]
2. El Diasty, W.S.; El Beialy, S.Y.; Mahdi, A.Q.; Peters, K.E. Geochemical characterization of source rocks and oils from northern Iraq: Insights from biomarker and stable carbon isotope investigations. *Mar. Pet. Geol.* **2016**, *77*, 1140–1162. [CrossRef]
3. Hakimi, M.H.; Ahmed, A.; Kahal, A.Y.; Hersi, O.S.; Al Faifi, H.J.; Qaysi, S. Organic geochemistry and basin modeling of Late Cretaceous Harshiyat Formation in the onshore and offshore basins in Yemen: Implications for effective source rock potential and hydrocarbon generation. *Mar. Pet. Geol.* **2020**, *122*, 104701. [CrossRef]
4. Lai, J.; Wang, G.; Wang, S.; Cao, J.; Li, M.; Pang, X.; Zhou, Z.; Fan, X.; Dai, Q.; Yang, L.; et al. Review of diagenetic facies in tight sandstones: Diagenesis, diagenetic minerals, and prediction via well logs. *Earth-Sci. Rev.* **2018**, *185*, 234–258. [CrossRef]
5. Zhao, C.; Jiang, Y.; Wang, L. Data-driven diagenetic facies classification and well-logging identification based on machine learning methods: A case study on Xujiahe tight sandstone in Sichuan Basin. *J. Pet. Sci. Eng.* **2022**, *217*, 110798. [CrossRef]
6. Wang, W.; Lin, C.; Zhang, X. Evaluation of sweet spots for a tight sandstone reservoir: A quantitative study of diagenesis in the fourth member of the Oligocene Huagang Formation, Xihu Depression, East China Sea Shelf Basin. *Mar. Pet. Geol.* **2024**, *163*, 106799. [CrossRef]

7. Wang, Z.Y.; Lu, S.F.; Zhou, N.W.; Liu, Y.C.; Lin, L.M.; Shang, Y.X.; Wang, J.; Xiao, G.S. Complementary testing and machine learning techniques for the characterization and prediction of middle Permian tight gas sandstone reservoir quality in the northeastern Ordos Basin, China. *Pet. Sci.* **2024**, *21*, 2946–2968. [CrossRef]
8. Yang, Y.T.; Li, W.; Ma, L. Tectonic and stratigraphic controls of hydrocarbon systems in the Ordos Basin: A multicycle cratonic basin in central China. *AAPG Bull.* **2005**, *89*, 255–269. [CrossRef]
9. Ju, Y.; Wang, W.; Jia, C.; Ren, Z.; He, D.; Chen, Z.; Farouq Ali, S.M.; Jiang, L. Inheritance and differentiation of the Ordos Basin under multidirectional convergence of plates. *Sci. Bull.* **2025**, *70*, 3110–3115. [CrossRef] [PubMed]
10. Tang, X.; Zhang, J.; Shan, Y.; Xiong, J. Upper Paleozoic coal measures and unconventional natural gas systems of the Ordos Basin, China. *Geosci. Front.* **2012**, *3*, 863–873. [CrossRef]
11. Wang, X.; Hou, L.; Li, J.; Yang, C.; Fan, L.; Chen, J.; Zhang, C.; Guo, J.; Tian, J.; Zhang, Y.; et al. Geochemical characteristics and gas source contributions of noble gases of the Sulige large tight gas field of Upper Paleozoic in Ordos Basin, China. *Front. Earth Sci.* **2022**, *10*, 889112. [CrossRef]
12. Wang, H.; Zhao, G.; Lu, S.; Li, L.; Zhang, W.; Liu, J. Investigation on hydrocarbon generation and expulsion potential by deep learning and comprehensive evaluation method: A case study of Hangjinqi area, Ordos Basin. *Mar. Pet. Geol.* **2022**, *144*, 105841. [CrossRef]
13. Wei, X.; Tang, J.; Song, H.; Chen, Y. Geochemical characteristics and hydrocarbon generation potential of Upper Paleozoic source rocks in Ganquan area, Ordos Basin. *Lithol. Reserv.* **2022**, *34*, 92–100. [CrossRef]
14. Fu, J.; Wei, X.; Luo, S.; Zuo, Z.; Zhou, H.; Liu, B.; Kong, Q.; Zhan, S.; Nan, J. Discovery and geological knowledge of the large deep coal-formed Qingyang Gas Field, Ordos Basin, NW China. *Pet. Explor. Dev.* **2019**, *46*, 1111–1126. [CrossRef]
15. Peng, H.; Wang, J.; Liu, C.; Zhao, H.; Huang, L.; Zhao, X.; Zhang, S.; Liang, C.; Wang, Z.; Cattò, S.; et al. Long-term and multiple stage exhumation of the Ordos Basin, western North China Craton: Insights from seismic reflection, borehole and geochronological data. *Earth-Sci. Rev.* **2023**, *238*, 104349. [CrossRef]
16. Bai, J.; Zhao, J.; Ren, Z.; Li, W.; Wang, K.; Li, X. Paleogeographic and sedimentary evolution of Meso–Neoproterozoic strata in the Ordos Basin, western North China Craton. *J. Pet. Sci. Eng.* **2022**, *215*, 110600. [CrossRef]
17. Liu, K.; Liu, J.; Huang, X. Coupled stratigraphic and petroleum system modeling: Examples from the Ordos Basin, China. *AAPG Bull.* **2021**, *105*, 1–28. [CrossRef]
18. Xu, L.; Cheng, Y.; Zhang, J.; Dang, W.; Liu, Y.; Tang, X.; Niu, J.; Tong, Z. Origin and isotopic fractionation of shale gas from the Shanxi Formation in the southeastern margin of Ordos Basin. *J. Pet. Sci. Eng.* **2022**, *208*, 109189. [CrossRef]
19. Wang, J.; Jiang, F.; Hu, Q.; Zhang, C.; Yang, X.; Mo, W.; Wang, X.; Qi, Z. A quantitative model and controlling factors of secondary pore development for tight sandstone reservoirs in the Carboniferous Benxi Formation, Ordos Basin, China. *Mar. Pet. Geol.* **2023**, *148*, 106034. [CrossRef]
20. Yang, Z.; Wang, A.; Meng, P.; Chen, M.; Guo, K.; Zhu, N. Combined use of in-reservoir geological records for oil-reservoir destruction identification: A case study in the Jingbian area (Ordos Basin, China). *Front. Earth Sci.* **2023**, *11*, 1133539. [CrossRef]
21. Liu, M.; Zhang, H.; Guo, H.; Zhao, W.; Wang, Y.; Shi, S.; Wang, Q.; Liu, J. The impact of marine influence on the hydrocarbon generation potential and process of Upper Paleozoic coal in the eastern Ordos Basin, China: Implications for unconventional gas exploration of coal measures. *Energy Fuels* **2024**, *38*, 12700–12717. [CrossRef]
22. Gao, H.; Wang, W. The newly discovered Yanchang gas field in the Ordos Basin, central China. *J. Earth Sci.* **2017**, *28*, 347–357. [CrossRef]
23. *GB/T 19145-2022*; Determination for Total Organic Carbon in Sedimentary Rock. Standards Press of China: Beijing, China, 2022.
24. *GB/T 18602-2012*; Rock Pyrolysis Analysis. Standards Press of China: Beijing, China, 2012.
25. *SY/T 5118-2021*; Determination of the Extract Content of Rock. Petroleum Industry Press: Beijing, China, 2022.
26. *SY/T 5125-2014*; Method of Identification Microscopically the Macerals of Kerogen and Indivision the Kerogen Type by Transmitted-Light and Fluorescence. Petroleum Industry Press: Beijing, China, 2015.
27. *SY/T 5124-2012*; Method of Determining Microscopically the Reflectance of Vitrinite in Sedimentary Rock. Petroleum Industry Press: Beijing, China, 2012.
28. *SY/T 5163-2018*; Analysis Method for Clay Minerals and Ordinary Non-Clay Minerals in Sedimentary Rocks by X-ray Diffraction. Petroleum Industry Press: Beijing, China, 2019.
29. *GB/T 13610-2020*; Analysis of Natural Gas Composition—Gas Chromatography. Standards Press of China: Beijing, China, 2020.
30. *SY/T 5238-2019*; Analysis Method for Carbon and Oxygen Isotopes in Organic Matter and Carbonate. Petroleum Industry Press: Beijing, China, 2019.
31. *SY/T 5523-2016*; Method for Analysis of Oilfield Water. Petroleum Industry Press: Beijing, China, 2016.
32. *SY/T 5735-2019*; Geochemical Method for Source Rock Evaluation. Petroleum Industry Press: Beijing, China, 2019.
33. Hakimi, M.H.; Abdullah, W.H.; Shalaby, M.R. Source rock characterization and oil generating potential of the Jurassic Madbi Formation, onshore East Shabowah oilfields, Republic of Yemen. *Org. Geochem.* **2010**, *41*, 513–521. [CrossRef]

34. Korkmaz, S.; Kara-Gülbay, R.; İztan, Y.H. Organic geochemistry of the Lower Cretaceous black shales and oil seep in the Sinop Basin, Northern Turkey: An oil–source rock correlation study. *Mar. Pet. Geol.* **2013**, *43*, 272–283. [CrossRef]
35. Zelilidis, A.; Tserolas, P.; Chamilaki, E.; Pasadakis, N.; Kostopoulou, S.; Maravelis, A.G. Hydrocarbon prospectivity in the Hellenic trench system: Organic geochemistry and source rock potential of Upper Miocene–Lower Pliocene successions in the eastern Crete Island, Greece. *Int. J. Earth Sci.* **2016**, *105*, 1859–1878. [CrossRef]
36. Maravelis, A.G.; Panagopoulos, G.; Piliotis, I.; Pasadakis, N.; Manoutsoglou, E.; Zelilidis, A. Pre-Messinian (sub-salt) source-rock potential on back-stop basins of the Hellenic Trench System (Messara Basin, Central Crete, Greece). *Oil Gas Sci. Technol.* **2016**, *71*, 6. [CrossRef]
37. Maravelis, A.G.; Chamilaki, E.; Pasadakis, N.; Vassiliou, A.; Zelilidis, A. Organic geochemical characteristics and paleodepositional conditions of an Upper Carboniferous mud-rich succession (Yagon Siltstone): Myall Trough, southeast Australia. *J. Pet. Sci. Eng.* **2017**, *158*, 322–335. [CrossRef]
38. Maravelis, A.G.; Perleros, K.; Papandropoulou, E.; Chamilaki, E.; Pasadakis, N.; Kalaitzidis, S.; Zelilidis, A. Petrographic and geochemical signatures of the Upper Permian Gondwana coals: Newcastle Coal Measures, Northern Sydney Basin, Australia. *Int. J. Coal Geol.* **2024**, *295*, 104628. [CrossRef]
39. Peters, K.E. Guidelines for evaluating petroleum source rock using programmed pyrolysis. *AAPG Bull.* **1986**, *70*, 318–329. [CrossRef]
40. Peters, K.E.; Cassa, M.R. Applied source rock geochemistry. In *The Petroleum System—From Source to Trap*; Magoon, L.B., Dow, W.G., Eds.; AAPG Memoir 60; American Association of Petroleum Geologists: Tulsa, OK, USA, 1994; pp. 93–120. [CrossRef]
41. Peters, K.E.; Walters, C.C.; Moldowan, J.M. *The Biomarker Guide*, 2nd ed.; Volume 2: Biomarkers and Isotopes in Petroleum Systems and Earth History; Cambridge University Press: Cambridge, UK, 2004. [CrossRef]
42. Yin, J.; Hu, P.; Guo, Y.; Li, Y.; Luo, S. Petrological characteristics and hydrocarbon generation of carbonate source rocks of the Permian Taiyuan Formation in central and eastern Ordos Basin, China. *Minerals* **2023**, *13*, 1058. [CrossRef]
43. Xiao, W.; Ji, H.; Huang, G. Geochemical characteristics and implications of hydrocarbon in source rocks of Chagan Sag, Yin'e Basin of Inner Mongolia. *Heliyon* **2023**, *9*, e13973. [CrossRef] [PubMed]
44. He, W.; Li, Z.; Li, C.; He, J.; Leng, J.; Sun, Z.; Liu, D.; Yang, S. Hydrocarbon generation, expulsion, and retention characteristics of the Permian Fengcheng shale and Lucaogou shale in the Junggar Basin: Implications for the exploration of lacustrine shale oil. *Front. Earth Sci.* **2025**, *12*, 1525983. [CrossRef]
45. Zhang, J.; Li, Y.; Liu, J.; Yan, X.; Li, L.; Shen, W. Modeling hydrocarbon generation of deeply buried Type III kerogen: A study on gas and oil potential of Lishui Sag, East China Sea Shelf Basin. *Front. Earth Sci.* **2021**, *8*, 609834. [CrossRef]
46. Dembicki, H., Jr. Three common source rock evaluation errors made by geologists during prospect or play appraisals. *AAPG Bull.* **2009**, *93*, 341–356. [CrossRef]
47. Guo, Q.; Jiang, S.; Wang, J.; Zhou, Q.; Gao, Y.; Ye, L.; Yin, J. Prediction of hydrocarbon source rock distribution using logging curves: A case study of $Es3^2$ source rock in Nanpu Sag, Huanghua Depression, Bohai Bay Basin. *Front. Earth Sci.* **2023**, *10*, 1097806. [CrossRef]
48. Cai, C.; Qiu, N.; Liu, N.; Li, Z.; Wang, Y.; Yu, Z.; Gao, T.; Jiao, Y. Geochemistry of formation waters and crude oils in the Shulu Sag, Bohai Bay Basin, NE-China, to assess quality and accumulation of hydrocarbons. *J. Pet. Sci. Eng.* **2022**, *210*, 110057. [CrossRef]
49. Humez, P.; Mayer, B.; Nightingale, M.; Becker, V.; Kingston, A.; Taylor, S.; Bayegnak, G.; Millot, R.; Kloppmann, W. Redox controls on methane formation, migration and fate in shallow aquifers. *Hydrol. Earth Syst. Sci.* **2016**, *20*, 2759–2777. [CrossRef]
50. Bordeleau, G.; Rivard, C.; Lavoie, D.; Lefebvre, R.; Malet, X.; Ladevèze, P. Geochemistry of groundwater in the Saint-Édouard area, Quebec, Canada, and its influence on the distribution of methane in shallow aquifers. *Appl. Geochem.* **2018**, *89*, 92–108. [CrossRef]
51. Wang, J.; Zhou, L.; Liu, J.; Zhang, X.; Luo, X.; Zhu, R.; Wu, Y.; Ren, Z.; Dick, J. Geochemistry of formation water and its implications for petroleum source rocks in the Fengcheng Formation, Mahu Depression, Xinjiang, China. *Front. Earth Sci.* **2022**, *9*, 774501. [CrossRef]
52. Sun, Z.; Yang, Z.; He, X.; Wan, C.; He, G.; Ren, Q.; Zhao, S.; Cheng, W.; Chen, S. Geochemical characteristics of formation water in carbonate reservoirs and its indication to hydrocarbon accumulation. *Geofluids* **2022**, *2022*, 6095178. [CrossRef]

Disclaimer/Publisher's Note: The statements, opinions and data contained in all publications are solely those of the individual author(s) and contributor(s) and not of MDPI and/or the editor(s). MDPI and/or the editor(s) disclaim responsibility for any injury to people or property resulting from any ideas, methods, instructions or products referred to in the content.